# MicroRNA-138-5p targets pro-apoptotic factors and favours neural cell survival

**Rodrigo M Maza**
Research Unit. Neuroprotection Group. National Hospital for Paraplegics
**Agata Silvan**
H Lundbeck A/S. Physiology and Symptoms
**Teresa Muñoz-Galdeano**
Research Unit. Neuroprotection Group. National Hospital for Paraplegics
**David Reigada**
Research Unit. Neuroprotection Group. National Hospital for Paraplegics https://orcid.org/0000-0001-9041-0705
**Ángela del Águila**
Cincinnati Children's Hospital Medical Center Division of Developmental Biology
**M. Asuncion Barreda-Manso**
Research Unit. Neuroprotection Group. National Hospital for Paraplegics
**Altea Soto**
Research Unit. Neuroprotection Group. National Hospital for Paraplegics
**Manuel Nieto-Diaz** ( mnietod@sescam.jccm.es )
Research Unit. Neuroprotection Group. National Hospital for Paraplegics https://orcid.org/0000-0002-7244-794X

**Research article**

**Keywords:** Neuroprotection, spinal cord injury, miR-based therapies, cell death

**Posted Date:** May 8th, 2020

**DOI:** https://doi.org/10.21203/rs.3.rs-26501/v1

# *MicroRNA-138-5p targets pro-apoptotic factors and favours neural cell survival*

Rodrigo M Maza[1], Agata Silván[1,2], Teresa Muñoz-Galdeano[1], David Reigada[1], Ángela del Águila[1,3], M. Asunción Barreda-Manso[1], Altea Soto[1], Manuel Nieto-Diaz[1*]

[1] Research Unit, Molecular Neuroprotection Group, National Hospital for Paraplegics, Toledo (Comunidad de Castilla La Mancha), Spain

Present adress:

[2] H. Lundbeck A/S, Physiology and Symptoms, Ottiliavej 9, 2500 Valby, Denmark and University of Copenhagen, Faculty of Health and Medical Sciences, Blegdamsvej 3B, 2200 Copenhagen, Denmark

[3] Division of Developmental Biology, Cincinnati Children´s Hospital Medical Center, Cincinnati, Ohio, United States of America

**E-mail adddresses:**

Rodrigo M Maza: rodrigom@sescam.jccm.es

Agata Silván: agsi@lundbeck.com

Teresa Muñoz-Galdeano: tmunozg@sescam.jccm.es

David Reigada: dreigada@sescam.jccm.es

Ángela del Águila: angela.delaguila@cchmc.org

M. Asunción Barreda-Manso: mbarreda@externas.sescam.jccm.es

Altea Soto: alteas@externas.sescam.jccm.es

***Corresponding Author**

Manuel Nieto-Diaz

Research Unit of the National Hospital for Paraplegics

Molecular Neuroprotection Group

National Hospital for Paraplegics (SESCAM)

Finca La Peraleda s/n

Toledo 45071, Spain

Tel: +34 925396834

Fax: + 34 925247745

E-mail: mnietod@sescam.jccm.es

## Abstract

**Background**

The central nervous system-enriched microRNA miR-138-5p becomes significantly downregulated after spinal cord injury (SCI). miR-138-5p modulates essential biological processes in the Central Nervous System (CNS). It also overcomes apoptosis by inhibiting the expression of proteins, including the effector CASP3, key in different cell death pathways. Therefore, we hypothesize that miR-138-5p downregulation following SCI underlies the overexpression of apoptotic genes and sensitizes neural cells to noxious stimuli. To confirm this hypothesis, this study aims a) to identify and validate miR-138-5p targets among the pro-apoptotic genes overexpressed following SCI; and b) to confirm that the miR-138-5p is able to modulate cell death in neural cells.

**Methods**

We employed computational tools to identify potential pro-apoptotic targets of miR-138-5p. Dysregulation of selected targets after SCI and its relationship to changes in miR-138-5p expression were analysed through qRT-PCR in a rat SCI model. Validation of the regulation of those apoptotic targets was carried out by luciferase reporter, qRT-PCR, and immunoblot assays in cultures of neural cell lines transfected with a mimetic of the microRNA. The functional effects of modifying the expression of miR-138-5p were later examined in cultures of the rat neural cell line C6 employing enzymatic assays to measure the activity of effector CASP3 and CASP7 together with MTT and flow cytometry assays to estimate cell death.

**Results**

Consensus among different algorithms identified 209 potential targets of miR-138-5p. A total of 176 of them become dysregulated after SCI, including proteins basic to apoptosis process such as CASP3 and CASP7, or BAK (Bcl-2 homologous antagonist/killer). Downregulation of miR-138-5p after SCI correlates with the overexpression of these three targets. Cell culture analyses confirm that miR-138-5p targets their 3'UTRs and reduces their expression after microRNA transfection. Transfection of miR-138-5p in C6 cell line results in a reduced effector caspase activity and protects cells from apoptotic stimulation.

**Conclusions**

Our results demonstrate that downregulation of miR-138-5p after SCI can be deleterious to spinal neural cells. A mixture of direct effects mediated by the upregulation of apoptotic targets and indirect effects related to the upregulation of cell cycle proteins can be expected.

**Keywords:** Neuroprotection, spinal cord injury, miR-based therapies, cell death

## Background

Injury to the spinal cord (SCI) triggers a barrage of damaging events that spread cell death to unaffected tissue [1]. Many of these noxious stimuli activate apoptosis -a highly regulated form of programmed cell death- among neural cells of the spinal cord during the following weeks [2–5]. The different apoptotic pathways converge in the activation of effector caspases, which are responsible for cleaving structural and functional proteins and leading to cell demise [6]. The noxious events triggered by SCI also alter gene expression in neural cells, including the overexpression of pro-apoptotic mediators such as Casp3 (coding for caspase-3 or CASP3 protein), Casp7 (caspase-7 or CASP7 protein), Bak1 (Bcl-2 homologous antagonist/killer or BAK protein), Bax, or Fas [7–9]. Post-transcriptional regulatory mechanisms contribute to orchestrate these gene expression changes [10,11]. Among them, studies have shown that microRNA dysregulation accompanies gene expression alterations in the injured spinal cord [12–14]. MicroRNAs are a class of highly conserved 20–24 nucleotides long noncoding RNA molecules that function as post-transcriptional regulators of cell state in physiological and pathological conditions [15]. They are highly expressed in the mammalian Central Nervous System (CNS), including the spinal cord, and their dysregulation is associated with neurodegenerative, psychiatric, and developmental diseases [16–18].

MicroRNA dysregulation after SCI has been proposed to contribute to spread cell death due to their targeting on key apoptotic genes. For example, SCI-downregulated miR-29b targets the overexpressed Bad, Bim, Noxa, and Puma [19], whereas the decreased level of miR-124 agrees with the overexpression of its target calpain-1 [20], and miR-137 downregulation agrees with calpain-2 and Casp3 overexpression [21].

Microarray and bioinformatics analyses in a rat model of contusive SCI [14] allowed us to identify additional dysregulated microRNAs that may also contribute to activating the apoptotic pathways. Among them, here we focus on miR-138-5p, a microRNA highly expressed in the CNS that becomes

significantly downregulated after SCI [12,14]. This microRNA controls the shape and size of dendritic spines in rat hippocampal neurons during development and thereby influences long-term memory [22]. Following injury, miR-138-5p participates in axon regeneration in peripheral nerve [23] and promotes neuroplasticity through the regulation of vimentin in the damaged spinal cord [24]. Outside the nervous system, miR-138-5p has attracted much attention in cancer research because it overcomes apoptotic cell death by simultaneous inhibition of multiple tumour suppressor pathways and pro-apoptotic genes, including the Casp3 [25]. Therefore, we hypothesize that, in addition to the previously described effects in the CNS, miR-138-5p downregulation after SCI underlies the overexpression of apoptotic genes and sensitizes neural cells to noxious stimuli. To confirm this hypothesis, this study aims a) to identify and validate miR-138-5p targets among the pro-apoptotic genes overexpressed following SCI; and b) to confirm that the miR-138-5p is able to modulate cell death in neural cells.

## Materials and Methods

### Computational prediction of miRNA targets and functional analysis

TargetScan7.1 (http://www.targetscan.org)[26], miRmap (http://mirmap.ezlab.org/)[27], miRanda (http://www.microrna.org)[28], and miRWalk2.0 (http://zmf.umm.uni-heidelberg.de/apps/zmf/mirwalk2)[29] miRNA target prediction softwares were employed to identify miR-138-5p response elements in rat messenger RNAs (mRNA). MiRWalk2.0 was employed as individual predictor to explore putative miRNA binding sites only within 3'UTR region. GEO2R web tool [30] was employed to identify those genes that become dysregulated in rat spinal cord during the first 10 days after injury according to high throughout gene expression data stored in the GEO datasets (https://www.ncbi.nlm.nih.gov/gds) references GSE464 (1, 3 and 7 days post-injury, [31]) and GSE69334 (3 and 10 days post-injury, [32]). To identify genes related to cell death, the obtained list of dysregulated genes was annotated using the Functional Annotation tool (default criteria) of the Database for Annotation, Visualization and Integrated Discovery (DAVID, http://david.abcc.ncifcrf.gov/)

[31]. Validated microRNA-target interactions were explored using miRTarBase6.0 database (http://mirtarbase.mbc.nctu.edu.tw/php/index.php; last accessed September 15th, 2019). In order to evaluate the stability of the target-miR-138-5p binding and the accessibility (i.e. how likely a region in a mRNA sequence is accessible for a miRNA to bind) of the mRNA secondary structure, the following tools were employed: 1) the mFold software (http://unafold.rna.albany.edu)[33], which was used to calculate the free energy (ΔG) of the predicted microRNA binding site and the 100 nucleotides flanking its 5' and 3' sides in the rat's 3'UTR mRNA of the target genes; 2) the PITA software (https://genie.weizmann.ac.il/)[34], setting the criterion of $\Delta\Delta G \leq -10$ kcal/mol and other parameters left to default. The accessibility of the miR-138-5p target site (ΔΔG) was calculated from the formula $\Delta\Delta G = \Delta G_{duplex} - \Delta G_{open}$, being $\Delta G_{open}$, the energy required to open the target mRNA secondary structure and $\Delta G_{duplex}$, the energy gained by the miRNA binding; 3) the miRmap prediction program (https://mirmap.ezlab.org/)[27], which computes the minimum free energy of this duplex, calculated from the Vienna RNA secondary structure library; and 4) the miRWalk3.0 prediction program (http://mirwalk.umm.uni-heidelberg.de/)[29], which calculates the RNA-duplex energy (ViennaRNA package)[35].

**Cell culture**

C6 rat brain glioma cells (cat#: CRL-2266, ATCC) were grown in RPMI-1640 medium (Gibco) supplemented with 10% fetal bovine serum (FBS; Gibco), 1% penicillin/streptomycin (Gibco) and 1% glutamine (Gibco). HEK293T human embryonic kidney cells (cat#: CRL-1573, ATCC) were grown in Dulbecco's modified Eagle's medium (Gibco) supplemented with 10% FBS and 1% penicillin/streptomycin. PC12 rat pheochromocytoma cells (cat#: CCL-1721, ATCC) were grown in Dulbecco's modified Eagle's medium (Gibco) supplemented with 10% Horse serum, 5% FBS, 1% penicillin/streptomycin, 1 mM sodium pyruvate (Gibco), 0.075% sodium bicarbonate, 1% Glutamine (Gibco), and 1X non-essential amino acids (Gibco). SH-SY5Y human neuroblastoma cells (cat#: CRL-2266, ATCC) were grown in a 1:1 combination of Minimum Essential Medium (Gibco) and Ham's F-12

nutrient mixture (Gibco), later supplemented with 10% FBS, 1% penicillin/streptomycin, 1 mM sodium pyruvate (Gibco) and 1X non-essential amino acids (Gibco). Cells were cultured in a humidified incubator at 37°C in an atmosphere containing 5% CO2.

**Dual luciferase reporter gene construction and 3'UTR luciferase reporter assays**

The complete 3'UTRs containing the predicted binding sites for rno-miR-138-5p of rat's Casp3 (position 1: 829-836 base pairs (bp), position 2: 881-887 bp), Casp7 (950-956 bp), and Bak1 (952-959 bp) were amplified by PCR using specific primers (table 1). The resulting products were subcloned into pGEM-T Easy vector (Promega) and then subcloned at the SacI or NheI and SalI sites downstream of the Firefly luciferase reporter gene of pmiRGLO (Promega). The 3'UTR of Fadd (Fas-associated protein with death domain) was subcloned to be employed as negative reporter construct. C6 or HEK293T cell lines, chosen on the basis of their consistent high protein expression of CASP3 and CASP7, and BAK (see Supplementary Material 5), were grown to 70% confluence in white 96-well plates. Then, cells were transfected with either 50 nM miR-138-5p mimic (miRIDIAN cat#: C-320369-05, Dharmacon) or 50 nM cel-miR-67 negative control microRNA (miRIDIAN microRNA mimic negative control#1 cat#: CN-001000-01; Dharmacon) and 200 ng/well of pmiRGLO containing each 3'UTR of the pro-apoptotic genes (or pmiRGLO empty as control) employing DharmaFECT Duo Transfection Reagent (Dharmacon). Firefly Luciferase and Renilla activities were measured 24 hours later with a plate reader (Infinite M200, Tecan) employing the Dual-GLO luciferase assay system (Promega) according to the manufacturer's protocol.

**Immunoblot assay**

Levels of CASP3 and CASP7, and BAK were analysed using standard immunoblot procedures. Briefly, cell lysates were incubated with radioimmunoprecipitation assay lysis buffer (RIPA) containing a complete EDTA-free protease inhibitor cocktail (Roche) and centrifugated (10000xg for 15 min at 4°C). Protein content was determined by the bicinchoninic acid method (BCA protein assay kit, ThermoFisher Scientific). A total of 50 µg of protein were resolved by SDS-PAGE, then electrophoretically transferred

to 0.2 µm polyvinylidene difluoride membrane (PVDF; Immobilon, Merk Millipore) and probed with antibodies aganist CASP3 (1:1000; Cell Signaling Technology, RRID:AB_10694681), CASP7 (1:1000; Cell Signaling Technology, RRID:AB_10831368), or BAK (1:1000; Cell Signaling Technology, RRID:AB_2290287) according to the manufacturer's protocol. β-tubulin antibody (1:10000; Sigma-Aldrich, RRID: AB_477580) was used as loading control. All antibodies were functionally validated by Cell Signalling Technology company. After incubation with the primary antibody, membranes were washed with TBS-Tween20 and incubated at RT for 1 hour with a horseradish peroxidase (HRP)-conjugated goat anti-rabbit secondary antibody (1:1000; ThermoFisher Scientific, RRID:AB_228341) or a HRP-conjugated goat anti-mouse secondary antibody (1:1000; ThermoFisher Scientific, RRID:AB_228307). Finally, HRP signal was developed using the SuperSignal West Pico Chemiluminescent detection system (Pierce, ThermoFisher Scientific), and measured using ImageScanner III and LabScan v6.0 software (GE Healthcare Bio-Sciences AB).

**MTT assay**

C6 cells were seeded overnight at a density of 20,000 cells per well in transparent 96-well plates and transfected with either miR-138-5p mimic or cel-miR-67 negative control using Dharmafect 1.0 (Dhamarcon). After 24 hours, cells were stimulated overnight with 0.3 µM staurosporine (STS; Sigma) or 127.5 µM etoposide (ETO; Sigma) or 1 mM L-glutamic acid (LGA; Sigma). Cells cultures were then incubated for 3 hours with (3-(4,5-dimethylthiazol-2-yl)-2,5-diphenyltetrazolium bromide) tetrazolium (MTT) in the medium at a final concentration of 0.5 mg/ml. Formazan crystals were dissolved by addition of 100 µl of HCl:Isopropanol (1:500) solution to each well followed by measurement of the absorbance at 570 nm (and 690 nm for backgrownd estimation) in a Infinite M200 plate reader.

**Measurement of CASP3 and CASP7 activity**

Briefly, C6 cells were seeded at a density of 20,000 cells per well in white 96-well plates and 24 hours after transfected with either miR-138-5p mimic or cel-miR-67 negative control microRNA employing Dharmafect 1.0 (Dhamarcon). The next day cell death was induced by treating the cultures with 0.3 µM

STS or 127.5 µM ETO overnight. Effector caspases activity was assessed 24 hours after, employing the luminescent Caspase-Glo® 3/7 assay kit (Promega), according to the manufacturer's instructions. Luminescence was measured in a Infinite M200 plate reader.

**Quantification of cell death using Flow Cytometry**

For cell death analysis, C6 cells were plated in duplicate for each transfection condition (cel-miR-67 negative control or miR-138-5p microRNAs) in p24 plates and cultured until reaching 50% confluence before transfection. Then, miRNA mimics were administered for transfection using Dharmafect 1.0 and, 24 hours later, cells were exposed to 127.5 µM ETO overnight. After detachment with 250 mM EDTA (ethylenediaminetetraacetic acid), apoptosis was analysed by Annexin V/SYTOX staining using the DY634 Annexin V Apoptosis Detection Kit (Immunostep) and SYTOX™ Green Nucleic Acid Stain (ThermoFisher Scientific) according to the manufacturer's instructions. Dot plots showing pulse width versus area was used to distinguish between single cells and aggregates. A total of 10,000 gated single events were collected using the FACS Canto II flow cytometry (BD Biosciences, Franklin Lakes, NJ, USA) and the FACS Diva 6.1 software (BD Biosciences) and analyzed with Flow Jo Software (Celeza GmbH, Olten, Switzerland) to determine the percentage of population stained with each dye. All flow cytometry procedures were carried out at the Flow Cytometry facility of the Research Unit from the Hospital Nacional de Parapléjicos (Toledo, Spain) with the assistance of its personnel.

**Surgical procedures**

Young adult (3 months old) female Wistar rats weighing approximately 200 g were employed for RNA extraction. Animals were housed in plastic cages in a temperature and humidity controlled room maintained on a 12:12 hours reverse light/dark cycle with free access to food and water. Animal experimental procedures were in accordance with the European Communities Council Directive (2010/63/EU) and were approved by the Hospital Nacional de Parapléjicos Animal Care and Use Committee (ref# 63/2010). Animals were divided into two groups: one group without surgery prior to

extraction (control) and one injured group (contusion). Animals were sacrificed at 3 and 7 days post-injury (dpi). 5 animals were randomly allocated in each time or control group using the sequence generator utility of the online random number generator random.org (https://www.random.org). SCI surgery followed the methodology described in Yunta and col. [14]. Briefly, animals were anaesthetized with intraperitoneal sodium pentobarbital at 40 mg/Kg (Dolethal, Vetoquinol) and underwent laminectomy at vertebral thoracic level 8 (T8). A 200 Kilodynes contusion was performed using an IH Spinal Cord Impactor (Precision System and Instrumentation, LLC). After surgery, animals were maintained by daily manual bladder emptying and by administration of Buprenorfine as analgesic (0.03 mg/Kg Buprex; Reckitt Benckiser Pharmaceuticals Limited), and enrofloxazine as antibiotic (0.4 mg/Kg Baytril; Bayer AG) for two days. At the defined times (1, 3, or 7dpi), animals were sacrificed by sodium pentobarbital over-dose and medullar fragments 1 cm long centered on the injury were extracted. Tissue fragments were maintained in RNAlater buffer (Qiagen) at -80ºC until RNA purification. Hind limb paralysis after injury was confirmed 1 or 2 days after the surgery using the Basso, Beattie, and Bresnahan 21-point locomotor score for rat models of SCI. We used a BBB value of 7 as the upper limit to include the animals in the gene expression analyses. Estabulation, surgeries, postoperative cares, and behavioural tests were carried out at the Animal facility of the Research Unit from the Hospital Nacional de Parapléjicos (Toledo, Spain) with the assistance of its personnel.

**qRT-PCR analysis**

miRNeasy Kit (Qiagen) was employed for isolation and purification of total RNA, including microRNAs, from rat spinal cord, as well as from C6, HEK293T, PC12 and SH-SY5Y cell lines. Total RNA concentration and purity (260/280 and 260/230 ratios) were estimated with a NanoDrop ND-1000 spectrophotometer (Thermo Scientific). RNA integrity was determined in animal samples according to the electropherogram and the derived RQI (RNA Quality Indicator) values obtained using the Experion microcapillary electrophoresis system (BioRad). Only samples with RQI values over 7.5, i.e. those with well-defined electropherograms, and with 260/280 ratios between 1.8 and 2.2 were employed.

To determine miR-138-5p expression, 10ng of total RNA was reverse-transcribed and amplified using TaqMan miRNA gene expression assay (TaqMan® MicroRNA assay #002284, Applied Biosystems) following manufacturer's protocols. The U6 small nuclear RNA served as an internal control (TaqMan® MicroRNA assay #001973, Applied Biosystems). For mRNA detection of Casp3, Casp7, and Bak1 transcripts, cDNA synthesis from 1µg of total RNA was subjected to random reverse transcription using Moloney Murine Leukemia Virus reverse transcriptase (M-MLV-RT; Invitrogen) and random primers (Roche). Gene expression was then measured using TaqMan Gene Expression Assays (Applied Biosystems) for Casp3 (#00563962), Casp7 (#01410847), and Bak1 (#01429084), employing 18S ribosomal RNA (#4333760) as housekeeping gene. Abundance of the microRNA and mRNAs of interest was measured in a thermocycler ABI Prism 7900 fast (Applied Biosystems) for 40 cycles of two steps: 15 s at 95°C plus 1 min at 60°C using the $2^{-\Delta\Delta Ct}$ method [36]. Briefly, the difference (ΔCt) between the cycle threshold of the target mRNA or miRNA and their respective endogenous loading controls -U6 small nuclear RNA for miRNAs and 18S ribosomal RNA for mRNA- was estimated together with its associated variance following the standard propagation of error method from Headrick and col. [37]. Then, we compared the ΔCt value from different times post-injury with the ΔCt from non-injured animals (0 dpi) to calculate the ΔΔCt and the correspondent fold increase ($2^{-\Delta\Delta Ct}$), indicating also the 95% confidence interval.

**Data analysis**

Statistical significance of the treatment effects was tested using paired or non-paired Student's t-test depending on the characteristics of the data. Normality and homocedasticity of the data were assessed using Shapiro-Wilkinson and Bartlett or F tests respectively, using the Shapiro.test, Bartlett.test, and var.test functions of R software. Sample size in the animal experiments were calculated employing the sensitivity function of G*Power 3.1 [38] to ensure a power level above 0.95 and a significance level below 0.05. Post-hoc analyses incorporating the actual within and between group variances confirmed a power level above 0.99. Data are expressed as mean±SEM or mean±SD as indicated in figure legends.

Statistical analyses and graphic design were conducted in Prism Software 5 (GraphPad Software Inc.) and R version 3.4.3 (https://www.R-project.org/)[39]. Differences were considered statistically significant when p-value was below 0.05.

## Results

### Predicting novel targets of miR-138-5p among the genes dysregulated after SCI

To explore the contribution of miR-138-5p dysregulation on the gene expression changes observed after SCI, we initially carried out an *in silico* analysis to predict potential targets of miR-138-5p. Since the various available programs can yield rather different predictions, we combined TargetScan 7.1, miRWalk 2.0, miRmap and miRanda- programs to search for rat miR-138-5p gene targets (Figure 1A). MiRWalk2.0 (green) identified a total of 1743 genes as predicted targets of miR-138-5p, whereas TargetScan (blue), miRmap (red) and miRanda (yellow) listed 2989, 2092 and 1159 genes respectively. A total of common 209 genes were identified by the four prediction programs (Supplementary Material 1). A comparison of this list with those genes differentially expressed after SCI according to GEO datasets GSE464 (1, 3 and 7dpi) and GSE69334 (3 and 10 dpi) revealed that 176 out of the 209 predicted miR-138-5p targets became dysregulated during the first days after injury (Figure 1A, see details in Supplementary Material 2 and 3). Functional annotation of this 176 genes using DAVID bioinformatics resources identified Gene Ontology terms for Biological Processes involving the apoptotic process or cell cycle including GO:0051402 (neuron apoptotic process), GO:2001238 (positive regulation of extrinsic apoptotic signaling pathway), GO:0051402 (neuron apoptotic process); GO:0097190 (apoptotic signaling pathway), GO:0006915 (apoptotic process), GO:0043066 (negative regulation of apoptotic process), GO:0043065 (positive regulation of apoptotic process), and GO:0007049 (cell cycle) (the full list is available in Supplementary Material 4). Among the miR-138-5p putative targets involved in apoptotic processes, we selected Casp3, Casp7, and Bak1 genes for detailed analysis, attending to their role in apoptotic cell death following SCI as well as to their values in the algorithm prediction scores. According to the employed prediction programs, rat Casp3 mRNA has two binding sites for miR-

138-5p in its 3'UTR, whereas Bak1 and Casp7 mRNA present only one site. Alignment of these putative sites in rat, mouse, and human sequences demonstrates the evolutionary conservation of Casp3 (site 2), Casp7, and Bak1 sites among mammalian species. No such conservation was observed for site 1 of Casp3 (Figure 1B). Exploration of miRTarBase6.0 (September 15th, 2019) database revealed that only Casp3 had been already experimentally validated as a target of human miR-138-5p.

Analyses of target site accessibility of the mRNA secondary structure further supported miR-138-5p targeting on the three predicted apoptotic targets (Figure 1C). Free energy (ΔG) values computed using mFold indicated that the miR-138-5p binding sites in the sequences of Casp3, Casp7 and Bak1 have a lower ΔG (mean ΔGCasp3= −12.7 kcal/mol; mean ΔGCasp7= −11.79 kcal/mol; mean ΔGBak1= −17.17 kcal/mol) than their corresponding 5' and 3' flanking regions, suggesting that miR-138-5p binding is particularly stable in these sites. Similarly, target site accessibility calculated using PITA software showed that the predicted interaction sites correspond to highly stable miRNA-mRNA duplexes formed by 8mer ($\Delta G_{duplex\ Casp3}$ = −21.8 kcal/mol; $\Delta G_{duplex\ Casp7}$ = −29.1 kcal/mol; and $\Delta G_{duplex\ Bak1}$ = −22.7 kcal/mol) with low overall energy requirements (ΔΔGCasp3 =−18.2 kcal/mol; ΔΔGCasp7 =−18.77 kcal/mol; and ΔΔGBak1 =−12.01 kcal/mol). MiRmap predictions on the minimum free energy of the miRNA-mRNA duplexes also supported a stable structure of the duplex of miR-138-5p and the three mRNA targets (ΔGbindingCasp3 =−22.65 kcal/mol, ΔGbindingCasp7 =−23.63 kcal/mol, and ΔGbindingBak1 =−19.93 kcal/mol). The minimal folding energy of the RNA-duplex calculated using miRWalk 3.0 software rendered similar results (ΔGbindingCasp3 =−22.0 kcal/mol, ΔGbindingCasp7 =−28.6 kcal/mol and ΔGbindingBak1 =−21.1 kcal/mol). Moreover, miRWalk3.0 showed as well a high accessibility of the duplexes of miR-138-5p with Casp3 (accessibility: site1=0.21, site2=0.01), Casp7 (accessibility=0.007), and Bak1 (accessibility=0.002). Taken together, bioinformatics approach agree that miR-138-5p has potential sites in the sequences of Casp3, Casp7, and Bak1, and therefore miR-138-5p can play a biologically relevant role in regulating their expression.

**Downregulation of miR-138-5p after SCI negatively correlates with the overexpression of Casp3, Casp7, and Bak1**

Previous studies based on murine SCI models [12,14] showed that miR-138-5p becomes downregulated 3 and 7 days after SCI. Present qPCR analysis of rat spinal cord samples confirmed the downregulation of miR-138-5p at 3 dpi and 7 dpi (Figure 2A). Additional qPCR analyses of the predicted miR-138-5p targets confirmed the previously described [7] overexpression of Casp3, Casp7, and Bak1 following SCI (Figure 2B). Comparison between miRNA and mRNA expression data suggests that the increase in target expression negatively correlates with the downregulation of miR-138-5p. Correlation was significant for Casp3 (Spearman correlation $r_s$: -0.8, $p<0.01$, Figure 2C) and Casp7 ($r_s$: -0.85, $p<0.01$, figure 2C) employing available paired data for miRNA and mRNA expression. Although a similar trend was observed when employing the mean daily values of miR-138-5p and Bak1 (see Figure 2C), lack of paired data and the number of available values (corresponding to 0, 3 and 7 dpi) precluded their analyses.

**miR-138-5p directly targets Casp3, Casp7, and Bak1 3'UTRs**

To experimentally validate the apoptotic targets of miR-138-5p predicted *in silico*, we carry out reporter assays as well as gene and protein expression analyses. In order to choose appropriate cell lines for these assays, we compared the endogenous levels of miR-138-5p, and CASP3, CASP7, and BAK proteins in different cell lines (Human: SH-SY5Y and HEK293T; Rat: PC12 and C6). We selected the human HEK293T and rat C6 cell lines for the following experiments due to their high CASP3, CASP7, and BAK protein expression level and their low to moderate endogenous expression of miR-138-5p (Supplementary Material 5). To evaluate whether miR-138-5p presents binding sites in Casp3, Casp7, and Bak1 3'UTRs, we prepared luciferase reporter constructs containing the rat wild-type 3'UTR of the three genes. We employed the 3'UTR of Fadd (apoptotic adaptor protein) with no predicted or validated miR-138-5p binding sites to control for unspecificity of reporter constructs. We co-transfected these constructs with miR-138-5p mimic or cel-miR-67 negative control (negative control)

into rat C6 or human HEK293T cells to perform a dual-luciferase reporter assay. Analysis of the normalized activity values (Firefly/Renilla) revealed no effect of miR-138-5p on the luciferase activity of the control construct (pmirGLO without 3'UTR subcloned) which yielded values similar to cultures treated with the negative control miRNA (Figure 3A), thus confirming that miR-138-5p did not alter luciferase activity. Conversely, co-transfection of the negative control miRNA with any of the 3'UTRs luciferase constructs in C6 cells significantly downregulated the luciferase activity (Figure 3A), suggesting that the expression of the three genes is subjected to an endogenous regulation. A similar reduction of luciferase activity was observed in human HEK293T cell cultures, except when co-transfecting Casp3 3'UTR construct (Figure 3B). Despite this endogenous downregulation of the three targets, transfection with the miR-138-5p mimic was able to further reduce the luciferase activity (compared to the negative control microRNA) in C6 cells when co-transfected with the 3'UTRs of Casp3 (Mean of differences±SD= 23.17±11.4 n=5, $t(4)=6.429$, $p=0.003$), Casp7 (17.88±10.584, n=4, $t(3)=5.506$ $p=0.018$), or Bak1 (16.89±12.58 n=4, $t(3)=4.36$, $p=0.022$), but not with Fadd (-6.5±26.9, n=3 $t(2)=0.643$, $p=0.17$). Luciferase activity was also significantly reduced, although to a lesser extent when HEK293T cells were co-transfected with the miR-138-5p mimetic and the luciferase construct of Casp3 (20±20.31 n=5, $t(4)=3.113$, $p=0.035$). Though no statistically significant, a similar trend was observed for the constructs of Casp7 (2.33±6.9, n=3, $t(2)=1.28$, $p=0.32$) and Bak1 (6.76±6.34, n=3, $t(2)=4.056$, $p=0.055$). As for C6 cells, the expression of Fadd construct remained unaffected by the transfection of the miR-138-5p mimetic (-1.58±27.6 n=3, $t(2)=1.28$, $p=0.86$) (Figure 3B). Altogether, the results from these reporter assays confirm that miR-138-5p regulates the 3'UTRs of Casp3, Casp7, and Bak1. These results also reveal that the endogenous and miR-138-5p regulation of the 3'UTRs of these proteins depends on cell type, being highly active in C6 neural cells compared to HEK293T kidney cells.

**miR-138-5p reduces the expression of Casp3, Casp7 and BAK**

To evaluate whether miR-138-5p modulates the cellular levels of Casp3, Casp7, and BAK, we employed RT-qPCR and immunoblot assays to measure the effect of transfecting miR-138-5p mimic on their

transcript and protein concentrations. C6 cell cultures were transiently transfected with either miR-138-5p or negative control microRNA mimic, and the mRNA levels of Casp3, Casp7, and Bak1 were measured by RT-qPCR. These experiments revealed that miR-138-5p mimic significantly decreased gene expression of Casp3, Casp7, and Bak1 (Figure 4A). As observed at mRNA level, when compared to transfection with negative control microRNA mimic, transfection of miR-138-5p led to a significant downregulation of the endogenous protein levels of CASP3 (56%±21, n=6, t(5)=5.06, p=0.004), CASP7 (48%±19, n=4, t(3)=5.31, p=0.013), and BAK (54%±22, n=6, t(5)=5.02, p=0.004)(Figure 4B). Therefore, as a whole, our data validated that miR-138-5p regulates the expression of its pro-apoptotic targets Casp3, Casp7, and BAK in C6 cells at both mRNA and protein level.

**miR-138-5p attenuates caspase-dependent apoptosis**

Since CASP3, CASP7, and BAK actively participate in apoptosis, we investigated whether miR-138-5p regulation of their expression also affects their activity in this cell death process. We focused these analyses on the effector CASP3 and CASP7, leaving BAK unanalyzed because its apoptotic activity ultimately relies on (and is reflected by) the cleavage and activation of both effector proteases [40]. For these functional studies, we first extended the immunoblot analysis of the pro-CASP3 and pro-CASP7 to examine the effects of transfecting miR-138-5p mimic in C6 cells under apoptotic conditions. It is well established that apoptotic stimulation leads to the proteolytic cleavage of the effector caspases and, concomitant, to the reduction in the levels of their proforms. Accordingly, stimulation of control C6 cells (i.e. transfected with negative control miRNA) with 350 µM ETO reduced the level of pro- pro-CASP3 and pro-CASP7 relative to unstimulated cells (pro-CASP3 reduction=46.59%±4.9, n=5; pro-CASP7 reduction=75.4%±13.8, n=4; see Figure 5A). ETO stimulation also reduced the levels of both pro-caspases when C6 cells were previously transfected with miR-138-5p mimics (pro-CASP3 reduction=18.02%±7.8, n=5; pro-CASP7 reduction=16.75%±1.8, n=4; Figure 5A). However, the reduction was significantly smaller than that measured in C6 cells transfected with the negative control miRNA (pro-CASP3: t(4)=3.577, p=0.023; pro-CASP7: t(3)=3.960, one-tailed p=0.029), indicating that

miR-138-5p modulation reduces caspase cleavage in C6 cells under apoptotic stimulation which ultimately should result in diminished activity of these proteases. To verify this hypothesis, we quantified the enzymatic activity of effector CASP3 and CASP7 in C6 cell cultures transfected with either miR-138-5p mimic or the negative control miRNA and exposed to apoptotic stimulation. As shown in Figure 5B, the enzymatic assay revealed that basal activity of the effector CASP3 and CASP7 was slightly but significantly lower when C6 cell cultures were transfected with the miR-138-5p mimic than when transfected with the negative control miRNA (ratio miR-138-5p mimic/negative control miRNA=0.9±0.005, n=3, t(2)=5.354, p=0.03). Upon apoptotic stimulation with either 127.5 µM ETO or 0.3 µM STS, caspases-3 and -7 activity was increased in C6 cells transfected with miR-138-5p mimic or negative control miRNA. However, transfection with miR-138-5p mimic led to a significantly minor increase of caspase activity after stimulation with either ETO (miR-138-5p mimic=1.16±0.1 *vs* negative control miRNA=1.4±0.1; n=4, t(3)=7.442, p=0.005) or STS (miR-138-5p mimic=1.86±0.69 *vs* negative control miRNA=2.35±0.68; n=4, t(3)=3.785, p=0.03). These results confirm that transfection with miR-138-5p mimics reduces the amount of pro-CASP3 and pro-CASP7 that becomes cleaved and, therefore, active.

Finally, we evaluated whether the reduction of the expression, cleavage and activity of CASP3 and CASP7 induced by the transfection of miR-138-5p mimics protects cells from apoptotic stimuli. To test this possibility, C6 cell cultures transfected for 24 hours with either negative control miRNA or miR-138-5p mimic were stimulated with 1 mM LGA, 127.5 µM ETO or 0.3 µM STS and their viability was analyzed using MTT assay. As illustrated in Figure 5C, transfection of miR-138-5p mimics significantly increased cell viability compared to transfection with negative control miRNA when cells were stimulated with LGA (miR-138-5p mimic=78%±14, negative control miRNA=45%±7, n=3, t(2)=7.189, p=0.01) or ETO (miR-138-5p mimic=86%±25, negative control miRNA=40%±10, n=3, t(2)=4.694, p=0.04). Viability followed a similar trend, though not significant when C6 cells were treated stimulated with 0.3 µM STS (miR-138-5p mimic=67%±35 *vs* negative control miRNA=30%±18, n=3, t(2)=3.723, p=0.06). We also

assayed cell viability by flow cytometry of C6 cultures transfected with either miR-138-5p mimic or negative control miRNAs and stimulated with 127.5 µM ETO using flow cytometry (Figure 5D). In agreement with MTT results, flow cytometry data indicates that the overexpression of miR-138-5p significantly increases cell viability compared to the overexpression of the negative control miRNA following treatment with ETO (miR-138-5p mimic=54.8%±5.9 *vs* negative control miRNA=44.5%±6.3, n=4, t(3)=4.78 p=0.0174). Therefore, altogether, present results indicate that overexpression of miR-138-5p favours C6 cell survival under apoptotic conditions by reducing the expression and pro-apoptotic activity of effector CASP3 and CASP7.

## Discussion

We designed the present study to search for evidence of the participation of miR-138-5p downregulation in the cell death processes that characterize SCI pathophysiology. MicroRNAs are known to regulate the identity, state, and fate of neural cells [15]. Not surprisingly, microRNA dysregulation accompanies multiple neurological pathologies [41], including SCI [42]. In search for microRNAs that could contribute to cell death progression during SCI pathophysiology, we identified the CNS-specific microRNA miR138-5p [43] as a potential candidate due to its dysregulation after SCI [12,14] and its targeting on the SCI-upregulated pro-apoptotic protein CASP3 [25]. miR-138-5p modulates essential biological processes in the CNS, including oligodendrocyte differentiation and myelin maintenance, or controlling dendritic spines morphogenesis of hippocampal neurons [22,44].

Before analyzing the effects of miR-138-5p dysregulation, we employed qRT-PCR to confirm the previously observed downregulation of this miRNA in a rat model of moderate contusive SCI. In agreement with the results from previous microarray analyses [12,14], our qRT-PCR data indicate that miR-138-5p reduces its expression in the spinal cord during the first week after injury. The decrease in miR-138-5p abundance may result from transcriptional changes in the neurons and oligodendrocytes that mainly express this miRNA [44], but also from the loss of these cells during the secondary injury. According to Bicker and colleagues [45], miR-138-5p expression in neurons is highly responsive to

pathologies and activity changes, suggesting that this miRNA and its targets may be involved in cellular processes that protect neurons from disturbance.

Once we confirmed the downregulation of miR-138-5p in our animal model of SCI, we explored how this dysregulation affects target expression in the damaged spinal cord, focusing on proteins involved in cell death. In a previous study [14], we already described that injury to the spinal cord leads to a significant enrichment of gene expression changes among miR-138-5p targets, which supposes clear evidence of the downregulation of this miRNA and indicates some of its potential effects in the damaged spinal cord. The *in silico* analyses carried out here extended the identified miR-138-5p targets to include additional cell death proteins among those upregulated after SCI according to available transcriptomic data [9,32]. Specifically, our *in silico* data identified the pro-apoptotic proteins CASP3, CASP7, and BAK as potential or validated miR-138-5p targets upregulated after SCI (see references above and [7,46–48]). Reporter and immunoblot assays confirmed miR-138-5p post-transcriptional regulation of CASP3 (previously shown by [25]), and established for the first time its regulation of CASP7 and BAK. Expression analyses revealed that the overexpression of the three targets in the injured spinal cord follows the downregulation of miR-138-5p, providing additional evidence of its regulation of the three pro-apoptotic targets. Previous studies have identified other miRNAs targeting them, such as miR-106b and miR-337-3p on CASP7 [49,50], miR-17-5p, miR-132-3p and miR-212-3p on Casp3 [50], and miR-125b on BAK [51]. Interestingly, except for miR-106b and miR-337-3p, all these miRNAs appear dysregulated during the first week after injury according to our prior microarray analyses [14] or similar studies [12,52] and, therefore, may cooperate to regulate the apoptotic pathway in the damaged spinal cord.

Apoptosis is a major mechanism of neural cell dismissal during the secondary damage of SCI [2]. This cell death process has been described to be induced by either downregulation of miRNAs aiming at pro-apoptotic genes, such as miR29b and the BH3 genes or upregulation of miRNAs that target anti-apoptotic genes, such as miR200c and FAP1 [53]. mir-138-5p's target BAK is a member of the BCL2

protein family that contributes to the activation of apoptosis through the permeabilization of the mitochondrial outer membrane to release apoptogenic factors, including cytochrome c [40]. The other two miR-138-5p targets, CASP3 and CASP7, are cysteine-aspartic acid proteases which, upon activation, execute the apoptotic program and play a central role in the extension of apoptosis after SCI [54,55]. It is our hypothesis that targeting on these targets will allow miR-138-5p to regulate cell death. In agreement, the results from our analyses demonstrate that the changes in miR-138-5p expression attenuate the enzymatic activity of CASP3 and CASP7 and conditions the execution of the apoptotic program. All these results suggest that miR-138-5p can be considered a neuroprotectant whose downregulation contributes to the secondary death of neural cells following SCI.

Even though the deleterious effects of miR-138-5p downregulation in the damaged CNS are explored here for the first time, the cytoprotective properties of this miRNA are well documented in astrocytes injured under ischemic conditions [56], glioblastoma [57], glioma stem cells [25], as well as in neural stem cells [58], pulmonary artery smooth muscle cells [59] and cardiomyocytes under hypoxia [60,61], and in microglial cells exposed to oxidative levels of $H_2O_2$ [62]. According to these studies, cytoprotection by miR-138-5p relies on its targeting and inhibition of the cell death-related genes Casp3, BLCAP and MXD1 [25], LCN2 [56,63], BIM [57], Mst-1 [64], and Mlk3 [61,62], or even in the inhibition of the JNK and p38MAPK pathways [58]. Some of these targets –including Casp3, Mst-1, BIM, and MLK3 (but also HIF-1α [65,66])– contribute to the cell death processes of secondary injury [67,68], suggesting that miR-138-5p can be considered a cytoprotectant whose downregulation contributes to extend neural cell death after SCI, as described by Tang and colleagues [63] for cerebral ischemia/reperfusion injury. In apparent opposition with this possibility, many cancer researchers consider miR-138-5p a tumour suppressor that becomes downregulated in different cancer processes, such as leukemia [69], lung cancer [70] and hepatocellular carcinoma [71]. Even within the nervous system, the ectopic expression of miR-138-5p in glioma multiforme cells seems to be tumour suppressive [72]. The antitumoral effects attributed to miR-138-5p mainly rely on its targeting on proliferative and cell cycle

proteins such as EZH2, E2F2, E2F3, CDK6, CCND3, or ABL1 [69,71,72] rather than on its direct induction of cell death. Interestingly, the antiproliferative and cell cycle arresting activity of miR-138-5p may be protective for neurons and oligodendrocytes, for which reentry in the cell cycle is linked to apoptosis after DNA damage in Alzheimer and other neurodegenerative diseases (see for review [73]). In fact, available evidence indicates that EZH2, E2F2, E2F3, and CCND3 become upregulated in the damaged spinal cord [74–76] where they can induce death among postmitotic neural cells during the secondary damage that follows SCI [9,74,77].

## Conclusions

Data from present and previous studies agree that downregulation of miR-138-5p after SCI can be deleterious to postmitotic neurons and oligodendrocytes through a mixture of direct effects mediated by the upregulation of apoptotic targets and indirect effects related to the upregulation of cell cycle proteins. Targeting of miR-138-5p on Sirt1, a regulator of autophagy initiation [78], may also contribute to the deleterious blockage of this process in neurons and oligodendrocytes following SCI (see [79] and references therein). In addition, miR-138-5p downregulation may also limit cytoprotective treatments due to its targeting on MDR1, a channel that confers drug resistance in cancer [80], which becomes upregulated in the damaged spinal cord to limit the effects of Riluzole [81]. Further studies will be neccessary to determine the precise contribution of miR-138-5p dysregulation on the activation of these cell death pathways after CNS injury. However, up to date, the available evidence suggests that miR-138-5p may be a valid neuroprotective target for SCI. Establishing the therapeutical value of miR-138-5p modulation for SCI will require additional information. On the one hand, it will be neccessary to carry out histological studies to identify which cells are expressing miR-138-5p in physiological conditions and which cells become dysregulated after injury both in animal models and particularly in humans. On the other hand, *in vivo* studies will be neccessary to evaluate the confirm of the therapeutical modulation of miR-138-5p in the damaged CNS.

## List of abbreviations

**Bak1/BAK:** Bcl-2 homologous antagonist/killer.

**BCA:** bicinchoninic acid assay.

**Casp3/CASP3:** Caspase-3.

**Casp7/CASP7:** Caspase-7.

**CNS:** Central Nervous System.

**EDTA:** Ethylenediaminetetraacetic acid.

**ETO:** Etoposide.

**FBS:** Fetal Bovine Serum.

**LGA:** L-Glutamic Acid.

**M-MLV-RT:** Moloney Murine Leukemia Virus reverse transcriptase.

**miR:** micro-ribonucleic acid/micro-RNA.

**RIPA:** Radioimmunoprecipitation assay buffer.

**SCI:** Spinal Cord Injury.

**STS:** Staurosporine.

## Declaration Section

## Statement of Ethics

All experimental procedures were in accordance with the European Communities Council Directive 2010/63/EU, Spanish Royal Decree 53/2013 (experimental animal use regulation) and Order ECC/566/

2015 (regulation of personnel formation in animal experimentation) and were approved by the Hospital Nacional de Paraplejicos Animal Care and Use Committee (project ref #153BCEEA/2016).

## Disclosure Statement

The authors have no conflicts of interest to declare

## Funding Sources

Research was funded by grants from the Fundación Tatiana Pérez de Guzmán el Bueno and the Council of Education, Culture and Sports of the Regional Government of Castilla La Mancha (Spain) and Co-financed by the European Union (FEDER) "A way to make Europe" (project reference SBPLY/17/000376). Altea Soto is funded by the Council of Education, Culture and Sports of the Regional Government of Castilla La Mancha (Spain). M. Asunción Barreda-Manso is funded by the Council of Health of the Regional Government of Castilla La Mancha (Spain).

## Author Contributions

Rodrigo M Maza was responsible for the conception and design of the experiments, the acquisition, analysis, and interpretation of the data. Agata Silván, Teresa Muñoz-Galdeano, David Reigada, Ángela del Aguila, M. Asunción Barreda-Manso, and Altea Soto contributed substantially to the acquisition, analysis, and interpretation of the data, and to draft and revise the manuscripts. Rodrigo M. Maza and Manuel Nieto-Díaz were responsible of drafting and revising the final version of the manuscript. All authors have revised and approved the final version of this article and express their agreement for all

aspects of the present work in ensuring that questions related to the accuracy or integrity of any part of the work are appropriately investigated and resolved.

All authors read and approved the final manuscript.

## Availability of data and materials

All data generated during this study are included in the published article and its supplementary information files.

## Acknowledgements

We thank the Fundacion del Hospital Nacional de Paraplejicos para la Investigacion y la Integracion (FUHNPAIIN) and the flow cytometry and animal facilities from the Research Unit of the Hospital Nacional de Paraplejicos (Toledo, Spain) for their technical and logistic support.

## References

1. Fehlings MG, Vaccaro AR, Boakye M. Essentials of Spinal Cord Injury: Basic Research to Clinical Practice. Thieme; 2012. 859 p.

2. Crowe MJ, Bresnahan JC, Shuman SL, Masters JN, Beattie MS. Apoptosis and delayed degeneration after spinal cord injury in rats and monkeys. Nat Med. 1997 Jan;3(1):73–6.

3. Grossman SD, Rosenberg LJ, Wrathall JR. Temporal–Spatial Pattern of Acute Neuronal and Glial Loss after Spinal Cord Contusion. Experimental Neurology. 2001 Apr;168(2):273–82.

4. Liu XZ, Xu XM, Hu R, Du C, Zhang SX, McDonald JW, et al. Neuronal and glial apoptosis after traumatic spinal cord injury. J Neurosci. 1997 Jul 15;17(14):5395–406.

5. Lou J, Lenke LG, Ludwig FJ, O'Brien MF. Apoptosis as a mechanism of neuronal cell death following acute experimental spinal cord injury. Spinal Cord. 1998 Oct;36(10):683–90.

6. Galluzzi L, Vitale I, Aaronson SA, Abrams JM, Adam D, Agostinis P, et al. Molecular mechanisms of cell death: recommendations of the Nomenclature Committee on Cell Death 2018. Cell Death Differ. 2018 Mar;25(3):486–541.

7. Aimone J, Leasure J, Perreau V, Thallmair M, Thechristopherreeveparalysisfounda. Spatial and temporal gene expression profiling of the contused rat spinal cord. Experimental Neurology. 2004 Oct;189(2):204–21.

8. Ahn YH, Bae Yeon Y, Lee G, Kang Mee K, Kang SK. Molecular insights of the injured lesions of rat spinal cords: Inflammation, apoptosis, and cell survival. Biochemical and Biophysical Research Communications. 2006 Sep;348(2):560–70.

9. Di Giovanni S, De Biase A, Yakovlev A, Finn T, Beers J, Hoffman EP, et al. In Vivo and in Vitro Characterization of Novel Neuronal Plasticity Factors Identified following Spinal Cord Injury. Journal of Biological Chemistry. 2005 Jan 21;280(3):2084–91.

10. Barbon A, Fumagalli F, Caracciolo L, Madaschi L, Lesma E, Mora C, et al. Acute spinal cord injury persistently reduces R/G RNA editing of AMPA receptors: AMPA R/G editing is reduced by SCI. Journal of Neurochemistry. 2010 Jul;114(2):397–407.

11.Nakae A, Nakai K, Tanaka T, Hosokawa K, Mashimo T. Serotonin 2C receptor alternative splicing in a spinal cord injury model. Neuroscience Letters. 2013 Jan;532:49–54.

12. Liu N-K, Wang X-F, Lu Q-B, Xu X-M. Altered microRNA expression following traumatic spinal cord injury. Experimental Neurology. 2009 Oct;219(2):424–9.

13. Strickland ER, Hook MA, Balaraman S, Huie JR, Grau JW, Miranda RC. MicroRNA dysregulation following spinal cord contusion: implications for neural plasticity and repair. Neuroscience. 2011 Jul;186:146–60.

14. Yunta M, Nieto-Díaz M, Esteban FJ, Caballero-López M, Navarro-Ruíz R, Reigada D, et al. MicroRNA Dysregulation in the Spinal Cord following Traumatic Injury. Di Giovanni S, editor. PLoS ONE. 2012 Apr 12;7(4):e34534.

15. Kosik KS. MicroRNAs and Cellular Phenotypy. Cell. 2010 Oct;143(1):21–6.

16. Bhalala OG, Srikanth M, Kessler JA. The emerging roles of microRNAs in CNS injuries. Nature Reviews Neurology. 2013 Jun;9(6):328–39.

17. Meza-Sosa KF, Valle-García D, Pedraza-Alva G, Pérez-Martínez L. Role of microRNAs in central nervous system development and pathology. Journal of Neuroscience Research. 2012 Jan;90(1):1–12.

18. Saugstad JA. MicroRNAs as Effectors of Brain Function with Roles in Ischemia and Injury, Neuroprotection, and Neurodegeneration. Journal of Cerebral Blood Flow & Metabolism. 2010 Sep;30(9):1564–76.

19. Liu X-J, Zheng X-P, Zhang R, Guo Y-L, Wang J-H. Combinatorial effects of miR-20a and miR-29b on neuronal apoptosis induced by spinal cord injury. Int J Clin Exp Pathol. 2015 Apr 15;8(4):3811–8.

20. Yi X, Jiang D. miR-124 mediated neuron apoptosis in spinal cord injury by targeting the 3' UTR end of calpain. Int J Clin Exp Pathol. 2016 Jun 15;9(6):5989–97.

21. Shen Q, Feng Z, Lu W. MicroRNA-137 inhibits apoptosis of neuron cells in injured spinal cord by targeting calpain 2. Int J Clin Exp Med. 2016 Aug 30;9(8):15796–803.

22. Siegel G, Obernosterer G, Fiore R, Oehmen M, Bicker S, Christensen M, et al. A functional screen implicates microRNA-138-dependent regulation of the depalmitoylation enzyme APT1 in dendritic spine morphogenesis. Nat Cell Biol. 2009 Jun;11(6):705–16.

23. Liu C-M, Wang R-Y, Saijilafu, Jiao Z-X, Zhang B-Y, Zhou F-Q. MicroRNA-138 and SIRT1 form a mutual negative feedback loop to regulate mammalian axon regeneration. Genes Dev. 2013 Jan 7;27(13):1473–83.

24. Qian B-J, You L, Shang F-F, Liu J, Dai P, Lin N, et al. Vimentin Regulates Neuroplasticity in Transected Spinal Cord Rats Associated with micRNA138. Molecular Neurobiology. 2015 Apr;51(2):437–47.

25. Chan XHD, Nama S, Gopal F, Rizk P, Ramasamy S, Sundaram G, et al. Targeting Glioma Stem Cells by Functional Inhibition of a Prosurvival OncomiR-138 in Malignant Gliomas. Cell Reports. 2012 Sep;2(3):591–602.

26. ..Agarwal V, Bell GW, Nam J-W, Bartel DP. Predicting effective microRNA target sites in mammalian mRNAs. Elife. 2015 Aug 12;4:101.

27. Vejnar CE, Blum M, Zdobnov EM. miRmap web: Comprehensive microRNA target prediction online. Nucleic Acids Research. 2013 Jul 1;41(Web Server issue):W165-8.

28. Betel D, Wilson M, Gabow A, Marks DS, Sander C. The microRNA.org resource: targets and expression. Nucleic Acids Research. 2008 Jan 1;36(Database issue):D149-53.

29. Dweep H, Gretz N. miRWalk2.0: a comprehensive atlas of microRNA-target interactions. Nature Publishing Group. 2015 Aug 1;12(8):697–697.

30. Barrett T, Wilhite SE, Ledoux P, Evangelista C, Kim IF, Tomashevsky M, et al. NCBI GEO: archive for functional genomics data sets—update. Nucleic Acids Research. 2012 Nov 26;41(D1):D991–5.

31. Di Giovanni S, Knoblach SM, Brandoli C, Aden SA, Hoffman EP, Faden AI. Gene profiling in spinal cord injury shows role of cell cycle in neuronal death. Ann Neurol. 2003 Apr;53(4):454–68.

32. Duan H, Ge W, Zhang A, Xi Y, Chen Z, Luo D, et al. Transcriptome analyses reveal molecular mechanisms underlying functional recovery after spinal cord injury. Proc Natl Acad Sci USA. 2015 Oct 27;112(43):13360–5.

33. Keith JM, editor. Bioinformatics [Internet]. Totowa, NJ: Humana Press; 2008 [cited 2020 Feb 6]. (Walker JM, editor. Methods in Molecular Biology™; vol. 453).

34. Kertesz M, Iovino N, Unnerstall U, Gaul U, Segal E. The role of site accessibility in microRNA target recognition. Nat Genet. 2007 Oct;39(10):1278–84.

35. Lorenz R, Bernhart SH, Höner zu Siederdissen C, Tafer H, Flamm C, Stadler PF, et al. ViennaRNA Package 2.0. Algorithms Mol Biol. 2011 Dec;6(1):26.

36. Livak KJ, Schmittgen TD. Analysis of Relative Gene Expression Data Using Real-Time Quantitative PCR and the 2−ΔΔCT Method. Methods. 2001 Dec;25(4):402–8.

37. Headrick TC. Statistical simulation: power method polynomials and other transformations. Boca Raton: Chapman & Hall/CRC; 2010. 166 p.

38. Faul F, Erdfelder E, Lang A-G, Buchner A. G*Power 3: A flexible statistical power analysis program for the social, behavioral, and biomedical sciences. Behavior Research Methods. 2007 May;39(2):175–91.

39. R Core Team. R: A language and environment for statistical computing. R Foundation for Statistical Computing, Vienna, Austria URL https://wwwR-project.org/. 2017;

40. Westphal D, Dewson G, Czabotar PE, Kluck RM. Molecular biology of Bax and Bak activation and action. Biochimica et Biophysica Acta (BBA) - Molecular Cell Research. 2011 Apr;1813(4):521–31.

41. Juźwik CA, S. Drake S, Zhang Y, Paradis-Isler N, Sylvester A, Amar-Zifkin A, et al. microRNA dysregulation in neurodegenerative diseases: A systematic review. Progress in Neurobiology. 2019 Nov;182:101664.

42. Nieto-Diaz M, Esteban FJ, Reigada D, Muñoz-Galdeano T, Yunta M, Caballero-López M, et al. MicroRNA dysregulation in spinal cord injury: causes, consequences and therapeutics. Front Cell Neurosci [Internet]. 2014 [cited 2019 Dec 9];8.

43. Obernosterer G. Post-transcriptional regulation of microRNA expression. RNA. 2006 May 18;12(7):1161–7.

44. Dugas JC, Notterpek L. MicroRNAs in Oligodendrocyte and Schwann Cell Differentiation. Dev Neurosci. 2011;33(1):14–20.

45. Bicker S, Lackinger M, Weiß K, Schratt G. MicroRNA-132, -134, and -138: a microRNA troika rules in neuronal dendrites. Cell Mol Life Sci. 2014 Oct;71(20):3987–4005.

46. Carmel JB, Galante A, Soteropoulos P, Tolias P, Recce M, Young W, et al. Gene expression profiling of acute spinal cord injury reveals spreading inflammatory signals and neuron loss. Physiological Genomics. 2001 Dec 21;7(2):201–13.

47. Citron BA, Arnold PM, Sebastian C, Qin F, Malladi S, Ameenuddin S, et al. Rapid Upregulation of Caspase-3 in Rat Spinal Cord after Injury: mRNA, Protein, and Cellular Localization Correlates with Apoptotic Cell Death. Experimental Neurology. 2000 Dec;166(2):213–26.

48. McEwen ML, Springer JE. A Mapping Study of Caspase-3 Activation Following Acute Spinal Cord Contusion in Rats. Journal of Histochemistry & Cytochemistry. 2005 Jul;53(7):809–19.

49. Hudson RS, Yi M, Esposito D, Glynn SA, Starks AM, Yang Y, et al. MicroRNA-106b-25 cluster expression is associated with early disease recurrence and targets caspase-7 and focal adhesion in human prostate cancer. Oncogene. 2013 Aug;32(35):4139–47.

50. Park J, Doseff A, Schmittgen T. MicroRNAs Targeting Caspase-3 and -7 in PANC-1 Cells. IJMS. 2018 Apr 16;19(4):1206.

51. Shi X-B, Xue L, Yang J, Ma A-H, Zhao J, Xu M, et al. An androgen-regulated miRNA suppresses Bak1 expression and induces androgen-independent growth of prostate cancer cells. Proceedings of the National Academy of Sciences. 2007 Dec 11;104(50):19983–8.

52. Hu J-Z, Huang J-H, Zeng L, Wang G, Cao M, Lu H-B. Anti-Apoptotic Effect of MicroRNA-21 after Contusion Spinal Cord Injury in Rats. Journal of Neurotrauma. 2013 Aug;30(15):1349–60.

53. . Yu DS, Lv G, Mei XF, Cao Y, Wang YF, Wang YS, et al. MiR-200c regulates ROS-induced apoptosis in murine BV-2 cells by targeting FAP-1. Spinal Cord. 2015 Mar;53(3):182–9.

54. Yu WR, Fehlings MG. Fas/FasL-mediated apoptosis and inflammation are key features of acute human spinal cord injury: implications for translational, clinical application. Acta Neuropathol. 2011 Dec;122(6):747–61.

55. Springer JE, Azbill RD, Knapp PE. Activation of the caspase-3 apoptotic cascade in traumatic spinal cord injury. Nat Med. 1999 Aug;5(8):943–6.

56. Deng Y, Chen D, Gao F, Lv H, Zhang G, Sun X, et al. Exosomes derived from microRNA-138-5p-overexpressing bone marrow-derived mesenchymal stem cells confer neuroprotection to astrocytes following ischemic stroke via inhibition of LCN2. J Biol Eng. 2019 Dec;13(1):71.

57. Stojcheva N, Schechtmann G, Sass S, Roth P, Florea A-M, Stefanski A, et al. MicroRNA-138 promotes acquired alkylator resistance in glioblastoma by targeting the Bcl-2-interacting mediator BIM. Oncotarget [Internet]. 2016 Mar 15 [cited 2019 Apr 15];7(11).

58. Zheng Z, Zhao B. Astragalus polysaccharide protects hypoxia-induced injury by up-regulation of miR-138 in rat neural stem cells. Biomedicine & Pharmacotherapy. 2018 Jun;102:295–301.

59. Li S, Ran Y, Zhang D, Chen J, Li S, Zhu D. microRNA-138 plays a role in hypoxic pulmonary vascular remodelling by targeting Mst1. Biochemical Journal. 2013 Jun 1;452(2):281–91.

60. Zhu H, Xue H, Jin Q-H, Guo J, Chen Y-D. MiR-138 protects cardiac cells against hypoxia through modulation of glucose metabolism by targetting pyruvate dehydrogenase kinase 1. Bioscience Reports. 2017 Dec 22;37(6):BSR20170296.

61. He S, Liu P, Jian Z, Li J, Zhu Y, Feng Z, et al. miR-138 protects cardiomyocytes from hypoxia-induced apoptosis via MLK3/JNK/c-jun pathway. Biochemical and Biophysical Research Communications. 2013 Nov;441(4):763–9.

62. Ren R, Chen SD, Fan J, Zhang G, Li JB. miRNA-138 regulates MLK3/JNK/MAPK pathway to protect BV-2 cells from H2O2-induced apoptosis. BLL. 2018;119(05):284–8.

63. Tang X-J, Yang M-H, Cao G, Lu J-T, Luo J, Dai L-J, et al. Protective effect of microRNA-138 against cerebral ischemia/reperfusion injury in rats. Experimental and Therapeutic Medicine. 2016 Mar;11(3):1045–50.

64. Li J, Chen Y, Qin X, Wen J, Ding H, Xia W, et al. MiR-138 downregulates miRNA processing in HeLa cells by targeting RMND5A and decreasing Exportin-5 stability. Nucleic Acids Research. 2013 Dec 31;42(1):458–74.

65. Xiaowei H, Ninghui Z, Wei X, Yiping T, Linfeng X. The experimental study of hypoxia-inducible factor-1a and its target genes in spinal cord injury. Spinal Cord. 2006; 44:9.

66. Song T, Zhang X, Wang C, Wu Y, Cai W, Gao J, et al. MiR-138 suppresses expression of hypoxia-inducible factor 1α (HIF-1α) in clear cell renal cell carcinoma 786-O cells. Asian Pac J Cancer Prev. 2011;12(5):1307–11.

67. Zhang M, Tao W, Yuan Z, Liu Y. Mst-1 deficiency promotes post-traumatic spinal motor neuron survival via enhancement of autophagy flux. J Neurochem. 2017 Oct;143(2):244–56.

68. Kole AJ, Annis RP, Deshmukh M. Mature neurons: equipped for survival. Cell Death Dis. 2013 Jun;4(6):e689–e689.

69. Xu C, Fu H, Gao L, Wang L, Wang W, Li J, et al. BCR-ABL/GATA1/miR-138 mini circuitry contributes to the leukemogenesis of chronic myeloid leukemia. Oncogene. 2014 Jan;33(1):44–54.

70. Gao Y, Fan X, Li W, Ping W, Deng Y, Fu X. miR-138-5p reverses gefitinib resistance in non-small cell lung cancer cells via negatively regulating G protein-coupled receptor 124. Biochemical and Biophysical Research Communications. 2014 Mar;446(1):179–86.

71. Wang W, Zhao L-J, Tan Y-X, Ren H, Qi Z-T. MiR-138 induces cell cycle arrest by targeting cyclin D3 in hepatocellular carcinoma. Carcinogenesis. 2012 Apr 30;33(5):1113–20.

72. Qiu S, Huang D, Yin D, Li F, Li X, Kung H, et al. Suppression of tumorigenicity by MicroRNA-138 through inhibition of EZH2-CDK4/6-pRb-E2F1 signal loop in glioblastoma multiforme. Biochimica et Biophysica Acta (BBA) - Molecular Basis of Disease. 2013 Oct;1832(10):1697–707.

73. Herrup K. Divide and Die: Cell Cycle Events as Triggers of Nerve Cell Death. Journal of Neuroscience. 2004 Oct 20;24(42):9232–9.

74. Wu J, Sabirzhanov B, Stoica BA, Lipinski MM, Zhao Z, Zhao S, et al. Ablation of the transcription factors E2F1-2 limits neuroinflammation and associated neurological deficits after contusive spinal cord injury. Cell Cycle. 2015 Dec 2;14(23):3698–712.

75. Yadav R, Weng H-R. EZH2 regulates spinal neuroinflammation in rats with neuropathic pain. Neuroscience. 2017 May;349:106–17.

76. Ji Y, Xiao F, Sun L, Qin J, Shi S, Yang J, et al. Increased expression of CDK11p58 and cyclin D3 following spinal cord injury in rats. Mol Cell Biochem. 2008 Feb;309(1–2):49–60.

77. Byrnes KR, Stoica BA, Fricke S, Di Giovanni S, Faden AI. Cell cycle activation contributes to post-mitotic cell death and secondary damage after spinal cord injury. Brain. 2007 Apr 5;130(11):2977–92.

78. Tian S, Guo X, Yu C, Sun C, Jiang J. miR-138-5p suppresses autophagy in pancreatic cancer by targeting *SIRT1*. Oncotarget [Internet]. 2017 Feb 14 [cited 2019 Dec 10];8(7).

79. Muñoz-Galdeano T, Reigada D, del Águila Á, Velez I, Caballero-López MJ, Maza RM, et al. Cell Specific Changes of Autophagy in a Mouse Model of Contusive Spinal Cord Injury. Front Cell Neurosci. 2018 Jun 12;12:164.

80. Zhao X, Yang L, Hu J, Ruan J. miR-138 might reverse multidrug resistance of leukemia cells. Leukemia Research. 2010 Aug;34(8):1078–82.

81. Dulin JN, Moore ML, Grill RJ. The Dual Cyclooxygenase/5-Lipoxygenase Inhibitor Licofelone Attenuates P-Glycoprotein-Mediated Drug Resistance in the Injured Spinal Cord. Journal of Neurotrauma. 2013 Feb;30(3):211–26.

## Figure Legends

**Table 1.** PCR primers employed in the subcloning of the 3'UTR regions of Casp3, Casp 7, and Bak1.

**Figure 1.** *Novel targets of miR-138-5p.* (A) Description and main data of the process of identification of novel apoptotic targets involved in SCI. Venn diagram of the miR-138-5p target genes predicted by miRmap, TargetScan, miRWalk and miRanda. Targets predicted by all four algorithms were compared with gene expression data from rat models of SCI. Common targets undergoing expression changes after SCI were analysed employing DAVID software. The table shows the miR-138-5p predicted targets related to the apoptotic process and their algorithm prediction scores. (B) Alignment of the seed regions of miR-138-5p with the 3'UTR of Casp3, Casp7, and Bak1 in human (Hsa), mouse (Mmu), and rat (Rno). (C) Accessibility for the predicted targets according to mFold, PITA, miRmap, and miRwalk 3.0.

**Figure 2.** *Expression of miR-138-5p negatively correlates with the expression of Casp3, Casp7, and Bak1 after SCI.* (A) Quantitative RT-PCR showing relative miR-138-5p expression in RNA isolated from spinal cord samples collected at the indicated days post-injury. The graph represents the $\Delta Ct(Ct_{miR138-5p}-Ct_{U6})$ from five independent experimental blocks ± 95% confidence interval (95% CI) and the table included the qRT-PCR data such as the mean ΔCt and the fold change $2^{-\Delta\Delta Ct}$ (the values in the parentheses are the limits in folds of the 95% CI; note that the target estimates are not in the center of this interval). Expression of miR-138-5p from each sample was normalized to the corresponding expression of the control gene snoRNA U6. (B) The tables show the mRNA expression of Casp3, Casp7 and Bak1 in the undamaged and the injured spinal cord as the mean ΔCt and the fold change $2^{-\Delta\Delta Ct}$

(values and limits in folds of the 95% CI) from six (Casp3 and Casp7) or three (Bak1) independent experimental blocks. The graph illustrates mRNA expression as $\Delta Ct(Ct_{target} - Ct_{18S}) \pm 95\%$ CI. Expression of miR-138-5p from each sample was normalized to the corresponding expression of the control gene 18S. * and ** denote significant differences ($p<0.05$ and $p<0.01$ respectively) relative to control undamaged samples according to an unpaired t-test. (C) Correlation between the expression of miR-138-5p and that of its predicted targets. Analyses were carried out employing the Spearman Correlation test due to the non-parametric nature of the experiment. Data employed for the correlation of Casp3 and Casp7 with miR-138-5p gene expression correspond to 9 individual samples extracted at 0, 3, and 7 dpi (n=3/time). Analysis of miR-138-5p and Bak1 correlation was based on the mean values of 0, 3, and 7 dpi due to the lack of paired analyses in the same samples.

**Figure 3.** *miR-138-5p directly targets the 3'UTR of Casp3, Casp7 and Bak1 genes*. Either C6 (A) or HEK293T (B) cell cultures were employed to measure the luciferase activity of the 3'UTR reporter constructs of the Casp3, Casp7, Bak1, Fadd and the control construct (Ctr; pmirGLO without 3'UTR subcloned). Cell cultures were transiently cotransfected with control or reporter constructs and miR-138-5p (white bars) or the negative control microRNA (black bars). Values correspond to the mean ± SD of at least three independent experiments. Luciferase activity of the different 3'UTR reporter constructs co-transfected with the negative control (Neg Ctr) was compared through a paired t-test (# $p<0.05$, relative to control construct). The effect of transfecting miR-138-5p mimetic relative to the negative control (Neg Ctr) in the luciferase activity of each co-transfected 3'UTR reporter construct was analysed using a paired t-test. * and ** indicate $p<0.05$ $p<0.01$ relative to its corresponding negative control.

**Figure 4.** *miR-138-5p inhibits the expression of caspase-3, caspase-7, and BAK. (*A) Gene expression data resulting from the RT-qPCR analysis of C6 cultures transiently transfected with miR-138-5p or the negative control mimics. The table details the mean ΔCt or fold change $2^{-\Delta\Delta Ct}$ (the values in the parentheses represent the 95% confidence interval; note that the interval is not centered for fold

change data). Comparison between expression values following miRNA-138-5p and negative control transfection in C6 cells was carried out through a paired t-test with ΔCt data (n=3 experiments). The graph underneath illustrates the effects of miR-138-5p mimic transfection on the gene expression of its apoptotic targets. (B) Protein expression differences between C6 cultures transiently transfected with miR-138-5p or the negative control mimics and analyzed using immunoblot and densitometry. Comparison between densitometry values was carried out through a paired t-test (n=4 experiments for CASP7; n=6 for CASP3 and BAK). The graph underneath shows the densitometry data of each apoptotic protein following transfection with miR-138-5p relative to their respective values after transfection with the negative control. * and ** indicate $p<0.05$ and $p<0.01$ relative to its corresponding negative control.

**Figure. 5.** *miR-138-5p attenuates caspase-dependent apoptosis.* (A) Protein expression of CASP3 and CASP7 in C6 cell cultures transiently transfected with miR-138-5p or the negative control mimic and stimulated with 350 µM ETO. The graph shows the densitometry of effector pro-caspases following transfection with miR-138-5p relative to the negative control (Ctr). ß-tubulin was used as the loading control and was used to normalize the densitometry values. Comparison between the densitometry values of unstimulated and ETO-stimulated cultures was carried out through a paired t-test (n=5 experiments for CASP3 and n=4 for CASP7). (B) Activity of effector CASP3 and CASP7 in C6 cell cultures transfected with miR-138-5p (white) or the negative control (black) mimic before and after apoptotic stimulation with 127.5 µM ETO or 0.3 µM STS. Values correspond to the mean ± SD of four independent experiments. miR-138-5p transfected cultures were compared with their corresponding negative control-transfected counterparts for each condition (* $p<0.05$). (C) Comparison of cell viability in C6 cell cultures transfected with miR-138-5p (white) and negative control (black) mimic was analysed using the MTT assay under different apoptotic stimulations (1 mM LGA, 127.5 µM ETO or 0.3 µM STS) in three independent experiments (*$P<0.05$). (D) A representative flow cytometry experiment showing the survival rate of C6 cell cultures transfected with miR-138-5p or negative

control mimic after 24 hours of 127.5 µM ETO stimulation. Cell cultures were stained with AnnexinV Dy634/SYTOX green and analysed using a flow cytometer. The graph summarizes the cell survival values (mean ± SD, n=4) of miR-138-5p (white) or negative control (black) transfected cells.

## Supplementary Material

**Supplementary Material 1**. (Suppl Material 1.xls) Full list of mir-138-5p targets predicted by TargetScan7.1 (http://www.targetscan.org), miRmap (http://mirmap.ezlab.org/), miRanda (http://www.microrna.org), and miRWalk2.0 (http://zmf.umm.uni-heidelberg.de/apps/zmf/mir walk2).

**Supplementary Material 2**. (Suppl Material 2.xls) List of genes that become dysregulated in the spinal cord during the first week after injury in rat models according to high throughout gene expression data stored in the GEO datasets GSE464 (1, 3 and 7 days post-injury) and GSE69334 (3 and 10 days post-injury).

**Supplementary Material 3**. (Suppl Material 3.xls) List of predicted miR-138-5p targets (Additional File 1) that become dysregulated after injury (Additional File 2).

**Supplementary Material 4**. (Suppl Material 4.xls) List of Gene Ontology terms for biological processes of the miR-138-5p targets dysregulated after SCI. GO terms related to apoptosis or cell cycle are highlighted.

**Supplementary Material 5**. (Suppl Material 5.pdf) Endogenous expression of miR-138-5p and CASP3, CASP7, and BAK in Hek293T, C6, SH-SY5Y and PC12 cell lines. MicroRNA expression was measured by qRT-PCR, whereas the protein expression of its targets was estimated by immunoblot (the image shown is a representative example). All experiments were carried out in triplicates.

# Figures

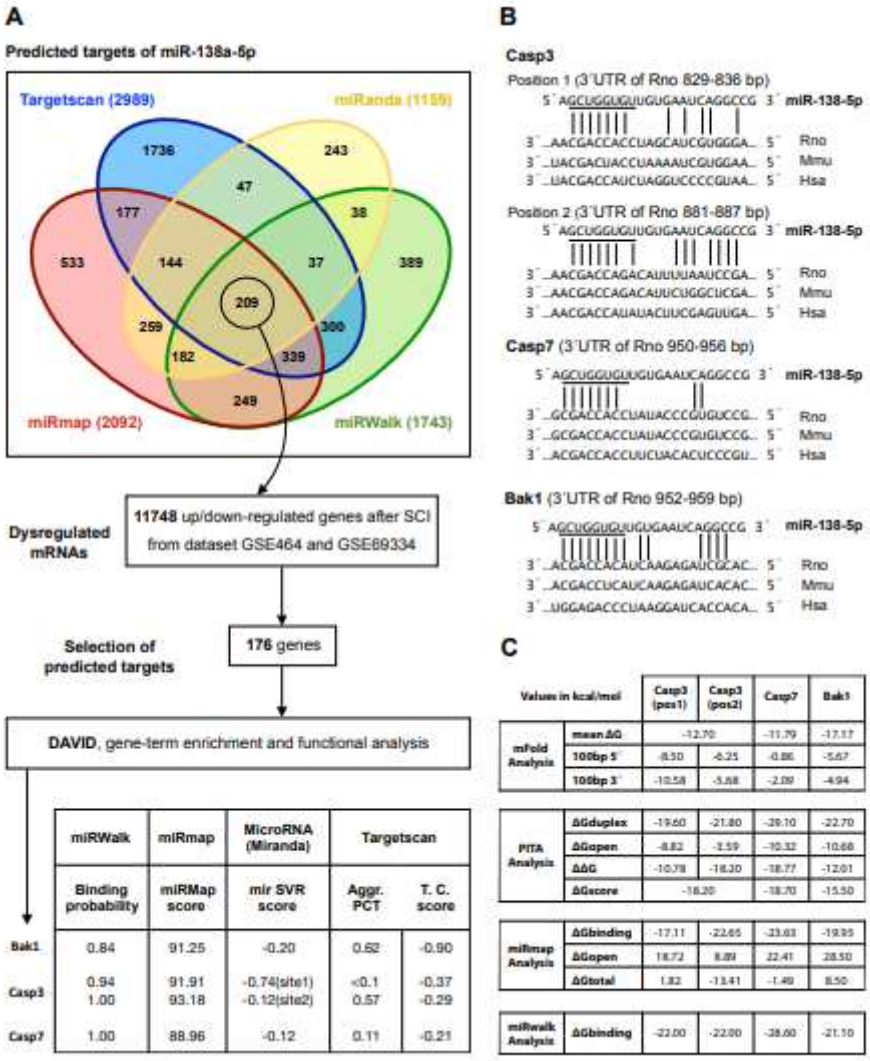


## Figure 1

Novel targets of miR-138-5p. (A) Description and main data of the process of identification of novel apoptotic targets involved in SCI. Venn diagram of the miR-138-5p target genes predicted by miRmap, TargetScan, miRWalk and miRanda. Targets predicted by all four algorithms were compared with gene expression data from rat models of SCI. Common targets undergoing expression changes after SCI were analysed employing DAVID software. The table shows the miR-138-5p predicted targets related to the apoptotic process and their algorithm prediction scores. (B) Alignment of the seed regions of miR-138-5p with the 3'UTR of Casp3, Casp7, and Bak1 in human (Hsa), mouse (Mmu), and rat (Rno). (C) Accessibility for the predicted targets according to mFold, PITA, miRmap, and miRwalk 3.0.

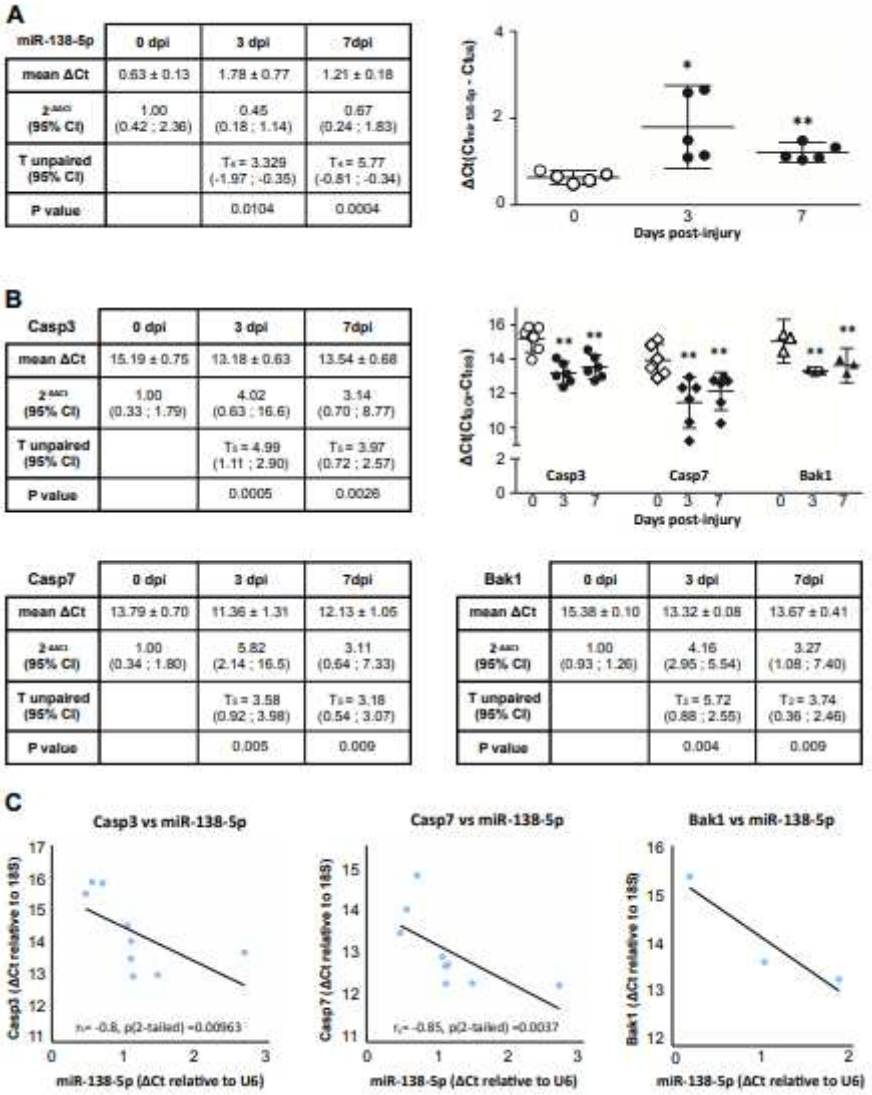


## Figure 2

Expression of miR-138-5p negatively correlates with the expression of Casp3, Casp7, and Bak1 after SCI. (A) Quantitative RT-PCR showing relative miR-138-5p expression in RNA isolated from spinal cord samples collected at the indicated days post-injury. The graph represents the ΔCt(CtmiR138 – 5p-CtU6) from five independent experimental blocks ± 95% confidence interval (95% CI) and the table included the qRT-PCR data such as the mean ΔCt and the fold change 2-ΔΔCt (the values in the parentheses are the limits in folds of the 95% CI; note that the target estimates are not in the center of this interval). Expression of miR-138-5p from each sample was normalized to the corresponding expression of the control gene snoRNA U6. (B) The tables show the mRNA expression of Casp3, Casp7 and Bak1 in the undamaged and the injured spinal cord as the mean ΔCt and the fold change 2-ΔΔCt 35 (values and limits in folds of the 95% CI) from six (Casp3 and Casp7) or three (Bak1) independent experimental blocks. The graph illustrates mRNA expression as ΔCt(Cttarget - Ct18S) ± 95% CI. Expression of miR-138-5p from each sample was normalized to the corresponding expression of the control gene 18S. * and ** denote significant differences ($p<0.05$ and $p<0.01$ respectively) relative to control undamaged samples

according to an unpaired t-test. (C) Correlation between the expression of miR138-5p and that of its predicted targets. Analyses were carried out employing the Spearman Correlation test due to the non-parametric nature of the experiment. Data employed for the correlation of Casp3 and Casp7 with miR-138-5p gene expression correspond to 9 individual samples extracted at 0, 3, and 7 dpi (n=3/time). Analysis of miR-138-5p and Bak1 correlation was based on the mean values of 0, 3, and 7 dpi due to the lack of paired analyses in the same samples

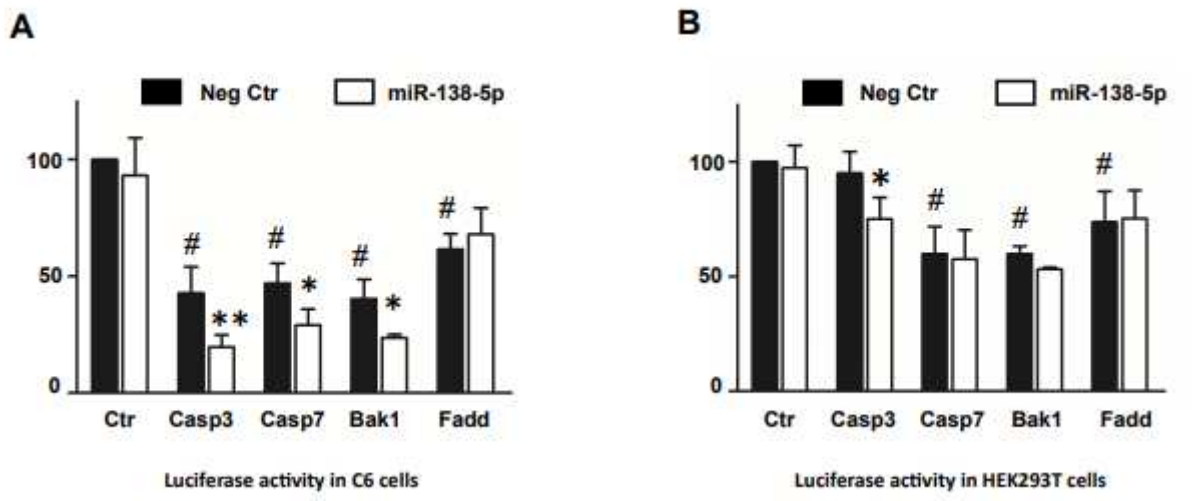


## Figure 3

miR-138-5p directly targets the 3'UTR of Casp3, Casp7 and Bak1 genes. Either C6 (A) or HEK293T (B) cell cultures were employed to measure the luciferase activity of the 3'UTR reporter constructs of the Casp3, Casp7, Bak1, Fadd and the control construct (Ctr; pmirGLO without 3'UTR subcloned). Cell cultures were transiently cotransfected with control or reporter constructs and miR138-5p (white bars) or the negative control microRNA (black bars). Values correspond to the mean ± SD of at least three independent experiments. Luciferase activity of the different 3'UTR reporter constructs co-transfected with the negative control (Neg Ctr) was compared through a paired t-test (# $p<0.05$, relative to control construct). The effect of transfecting miR-138-5p mimetic relative to the negative control (Neg Ctr) in the luciferase activity of each co-transfected 3'UTR reporter construct was analysed using a paired t-test. * and ** indicate $p<0.05$ $p<0.01$ relative to its corresponding negative control.

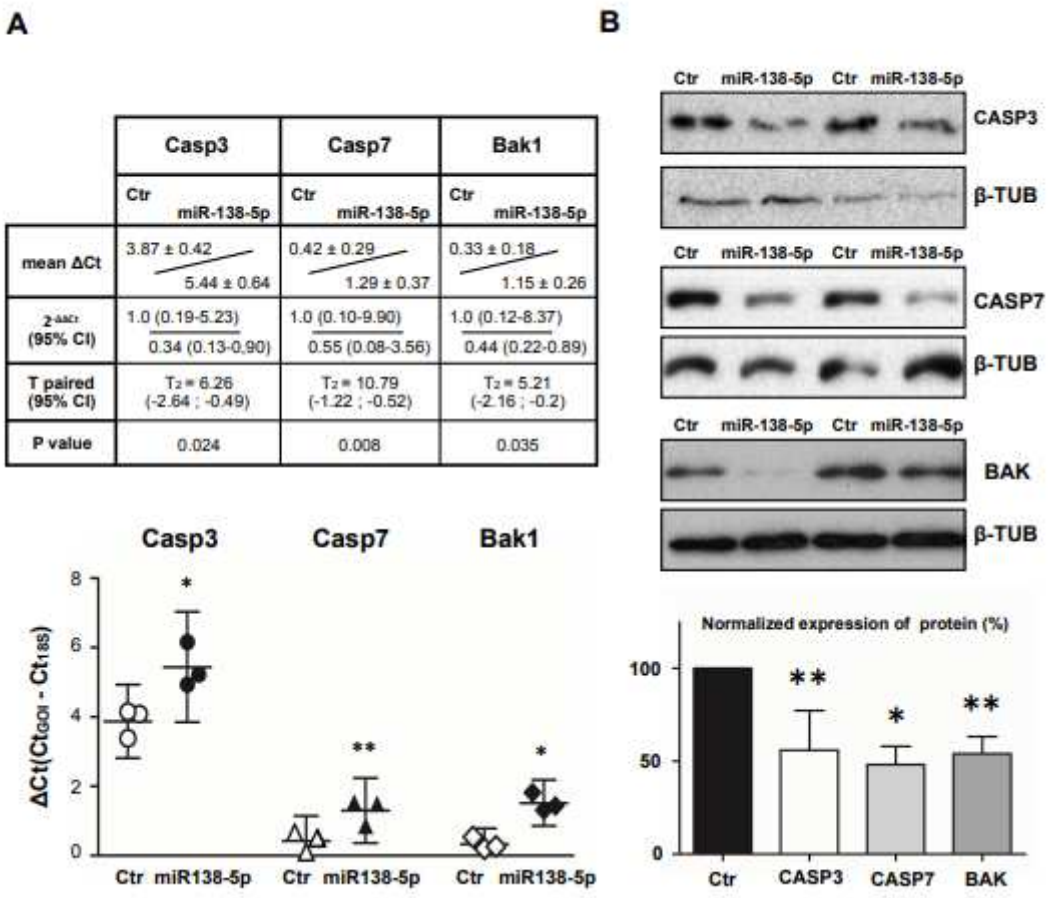


## Figure 4

miR-138-5p inhibits the expression of caspase-3, caspase-7, and BAK. (A) Gene expression data resulting from the RT-qPCR analysis of C6 cultures transiently transfected with miR-138-5p or the negative control mimics. The table details the mean ΔCt or fold change 2-ΔΔCt (the values in the parentheses represent the 95% confidence interval; note that the interval is not centered for fold 36 change data). Comparison between expression values following miRNA-138-5p and negative control transfection in C6 cells was carried out through a paired t-test with ΔCt data (n=3 experiments). The graph underneath illustrates the effects of miR-138-5p mimic transfection on the gene expression of its apoptotic targets. (B) Protein expression differences between C6 cultures transiently transfected with miR-138-5p or the negative control mimics and analyzed using immunoblot and densitometry. Comparison between densitometry values was carried out through a paired t-test (n=4 experiments for CASP7; n=6 for CASP3 and BAK). The graph underneath shows the densitometry data of each apoptotic protein following transfection with miR-138-5p relative to their respective values after transfection with the negative control. * and ** indicate $p<0.05$ and $p<0.01$ relative to its corresponding negative control.

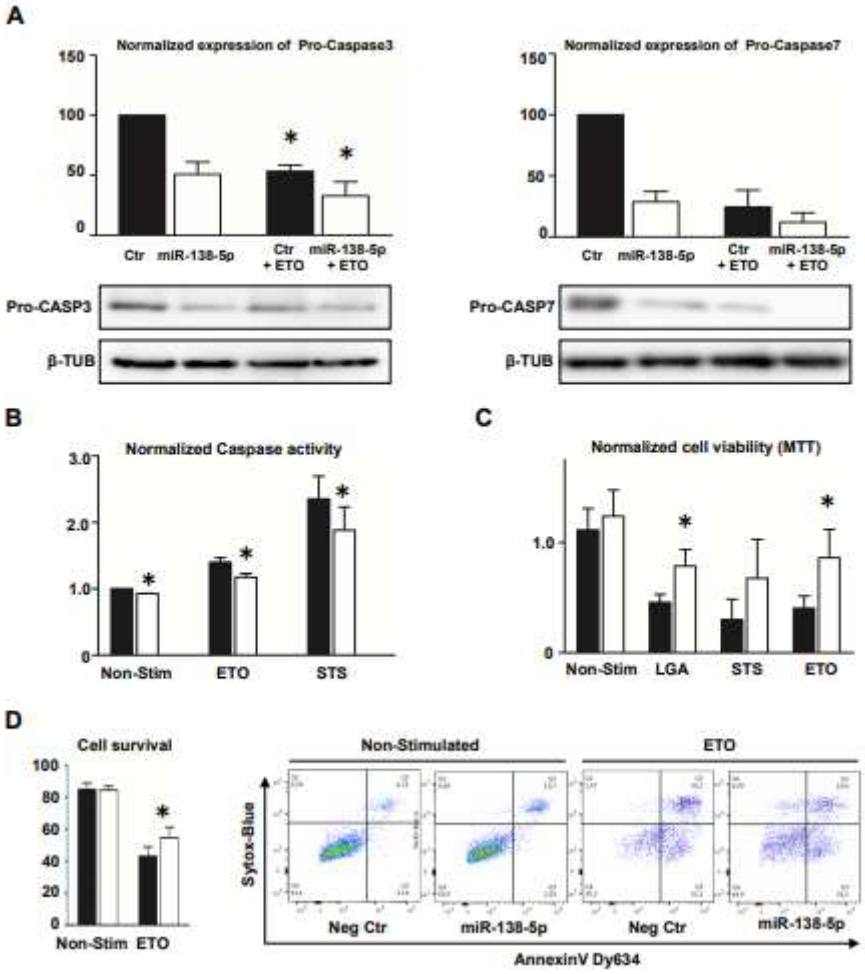


## Figure 5

miR-138-5p attenuates caspase-dependent apoptosis. (A) Protein expression of CASP3 and CASP7 in C6 cell cultures transiently transfected with miR-138-5p or the negative control mimic and stimulated with 350 µM ETO. The graph shows the densitometry of effector pro-caspases following transfection with miR-138-5p relative to the negative control (Ctr). ß-tubulin was used as the loading control and was used to normalize the densitometry values. Comparison between the densitometry values of unstimulated and ETO-stimulated cultures was carried out through a paired t-test (n=5 experiments for CASP3 and n=4 for CASP7). (B) Activity of effector CASP3 and CASP7 in C6 cell cultures transfected with miR-138-5p (white) or the negative control (black) mimic before and after apoptotic stimulation with 127.5 µM ETO or 0.3 µM STS. Values correspond to the mean ± SD of four independent experiments. miR-138-5p transfected cultures were compared with their corresponding negative control-transfected counterparts for each condition (* $p<0.05$). (C) Comparison of cell viability in C6 cell cultures transfected with miR-138-5p (white) and negative control (black) mimic was analysed using the MTT assay under different apoptotic stimulations (1 mM LGA, 127.5 µM ETO or 0.3 µM STS) in three independent experiments (*$P <0.05$). (D) A representative flow cytometry experiment showing the survival rate of C6 cell cultures transfected with miR-138-5p or negative 37 control mimic after 24 hours of 127.5 µM ETO stimulation. Cell cultures were stained with AnnexinV Dy634/SYTOX green and analysed using a flow cytometer. The graph summarizes

the cell survival values (mean ± SD, n=4) of miR-138-5p (white) or negative control (black) transfected cells.

## Supplementary Files

This is a list of supplementary files associated with this preprint. Click to download.

- SupplMaterial1.xlsx
- SupplMaterial5.pdf
- SupplMaterial1.xlsx
- SupplMaterial2.xlsx
- SupplMaterial4.xlsx
- SupplMaterial3.xlsx
- SupplMaterial2.xlsx
- SupplMaterial3.xlsx
- SupplMaterial5.pdf
- Table1.pdf
- SupplMaterial4.xlsx
- Table1.pdf